Advances in Chemical Physics
Stuart A. Rice and Aaron R. Dinner, Series Editors

Advances in Chemical Physics

Volume 155

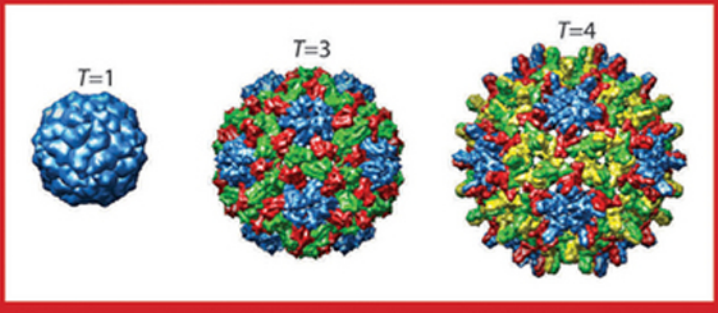

Edited by
Stuart A. Rice
Aaron R. Dinner

WILEY

ADVANCES IN CHEMICAL PHYSICS

VOLUME 155

EDITORIAL BOARD

ADVANCES IN CHEMICAL PHYSICS

VOLUME 155

Edited by

STUART A. RICE

Department of Chemistry
and
The James Franck Institute
The University of Chicago
Chicago, Illinois

AARON R. DINNER

Department of Chemistry
and
The James Franck Institute
The University of Chicago
Chicago, Illinois

WILEY

Published by John Wiley & Sons, Inc., Hoboken, New Jersey.
Published simultaneously in Canada.

Library of Congress Catalog Number: 58-9935

ISBN: 978-1-118-75577-8

Printed in the United States of America

10 9 8 7 6 5 4 3 2 1

CONTRIBUTORS TO VOLUME 155

VISHAL AGARWAL, Department of Chemical Engineering, University of California, Santa Barbara, CA 93106, USA

ALAN ASPURU-GUZIK, Department of Chemistry and Chemical Biology, Harvard University, 12 Oxford Street, Cambridge, MA 02138, USA

RYAN BABBUSH, Department of Chemistry and Chemical Biology, Harvard University, 12 Oxford Street, Cambridge, MA 02138, USA

MICHAEL F. HAGAN, Department of Physics, Brandeis University, MS057, Waltham, MA 02454, USA

TOSHIKO ICHIYE, Department of Chemistry, Georgetown University, Washington, DC 20057-1227, USA

PAVEL JUNGWIRTH, Institute of Organic Chemistry and Biochemistry, Academy of Sciences of the Czech Republic, Flemingovo nám. 2, 16610 Prague 6, Czech Republic

WILLIAM MACREADY, D-Wave Systems, Inc., 100-4401 Still Creek Drive, Burnaby, British Columbia V5C 6G9, Canada

BRYAN O'GORMAN, Department of Chemistry and Chemical Biology, Harvard University, 12 Oxford Street, Cambridge, MA 02138, USA

ALEJANDRO PERDOMO-ORTIZ, Department of Chemistry and Chemical Biology, Harvard University, 12 Oxford Street, Cambridge, MA 02138, USA; NASA Ames Quantum Laboratory, Ames Research Center, Moffett Field, CA 94035, USA

BARON PETERS, Department of Chemical Engineering; Department of Chemistry and Biochemistry, University of California, Santa Barbara, CA 93106, USA

FRANK UHLIG, Institute of Organic Chemistry and Biochemistry, Academy of Sciences of the Czech Republic, Flemingovo nám. 2, 16610 Prague 6, Czech Republic

ROBERT VÁCHA, National Centre for Biomolecular Research, Faculty of Science and CEITEC—Central European Institute of Technology, Masaryk University, Kamenice 5, 62500 Brno-Bohunice, Czech Republic

PREFACE TO THE SERIES

Advances in science often involve initial development of individual specialized fields of study within traditional disciplines followed by broadening and overlap, or even merging, of those specialized fields, leading to a blurring of the lines between traditional disciplines. The pace of that blurring has accelerated in the past few decades, and much of the important and exciting research carried out today seeks to synthesize elements from different fields of knowledge. Examples of such research areas include biophysics and studies of nanostructured materials. As the study of the forces that govern the structure and dynamics of molecular systems, chemical physics encompasses these and many other emerging research directions. Unfortunately, the flood of scientific literature has been accompanied by losses in the shared vocabulary and approaches of the traditional disciplines, and there is much pressure from scientific journals to be ever more concise in the descriptions of studies, to the point that much valuable experience, if recorded at all, is hidden in supplements and dissipated with time. These trends in science and publishing make this series, *Advances in Chemical Physics*, a much needed resource.

The *Advances in Chemical Physics* is devoted to helping the reader obtain general information about a wide variety of topics in chemical physics, a field that we interpret very broadly. Our intent is to have experts present comprehensive analyses of subjects of interest and to encourage the expression of individual points of view. We hope that this approach to the presentation of an overview of a subject will both stimulate new research and serve as a personalized learning text for beginners in a field.

STUART A. RICE
AARON R. DINNER

CONTENTS

MODELING VIRAL CAPSID ASSEMBLY

MICHAEL F. HAGAN

Department of Physics, Brandeis University, MS057, Waltham, MA 02454, USA

Advances in Chemical Physics, Volume 155, First Edition. Edited by Stuart A. Rice and Aaron R. Dinner.

I. INTRODUCTION

The formation of a virus is a marvel of natural selection. A large number (60–10,000) of protein subunits and other components assemble into complete, reproducible structures, often with extreme fidelity, on a biologically relevant time scale. Viruses play a role in a significant portion of human diseases, as well as those of other animals, plants, and bacteria. Thus, it is of great interest to understand their formation process, with the goal of developing novel antivirus therapies that can block it, or alternatively to re-engineer viruses as drug delivery vehicles that can assemble around their cargo and disassemble to deliver it without requiring explicit external control. More fundamentally, learning the factors that make viral assembly so robust could advance the development of self-assembling nanostructured materials.

This chapter focuses on the use of theoretical and computational modeling to understand the viral assembly process. We begin with brief overviews of virus structure, assembly, and the experiments used to characterize the assembly process (Section I). We next perform an equilibrium analysis of the assembly of empty protein shells in Section II. In Section III, we then present a simple mathematical representation of the assembly process and its relevant timescales, followed by several types of modeling approaches that have been used to analyze and predict *in vitro* assembly kinetics. We then extend the equilibrium and dynamical approaches to consider the co-assembly of capsid proteins with RNA or other polyanionic cargoes in Section IV. Finally, we conclude with some of the important open questions and ways in which modeling can make a stronger connection with experiments.

In the interests of thoroughly examining the capsid assembly process, this chapter will not consider a number of interesting topics such as the structural dynamics of complete capsids (e.g., [1–4]), capsid swelling or maturation transitions (e.g., [5–13]), mechanical probing of assembled capsids (e.g., [10,14–24]), motor-driven packaging of double-stranded DNA (dsDNA) into assembled procapsids (e.g., [25–31], reviewed in Refs. [32–34]), or the conformations of dsDNA inside capsids (e.g., [35–37]).

A. Virus Anatomies

Viruses consist of at least two types of components: the genome, which can be DNA or RNA and can be single or double stranded, and a protein shell called a capsid that surrounds and protects the fragile nucleic acid. Viruses vary widely in complexity, ranging from satellite tobacco mosaic virus (STMV), whose 1063-nucleotide genome encodes for two proteins including the capsid protein [38], to the giant Megavirus, with a 1,259,197 bp genome encoding for 1120 putative

proteins [39], that is larger than some bacterial genomes and encased in two capsids and a lipid bilayer. Viruses such as Megavirus that acquire a lipid bilayer coating from the plasma membrane or an interior cell compartment of the host organism are known as ''enveloped'' viruses, whereas viruses such as STMV that present a naked protein exterior are termed ''nonenveloped.'' Since Harrison et al. achieved the first atomic-resolution structure of tomato bushy stunt virus (TBSV) in 1978 [40], structures of numerous virus capsids have been revealed to atomic resolution by X-ray crystallography and/or cryo-electron microscopy (cryo-EM) images. An extensive collection of virus structures can be found at the VIPERdb virus particle explorer web site (http://viperdb.scripps.edu) [41].

The requirement that the viral genome be enclosed in a protective shell severely constrains its length and hence the number of protein sequences that it can encode. As first proposed by Crick and Watson [42], virus capsids are therefore comprised of numerous copies of one or a few protein sequences, which are usually arranged with a high degree of symmetry in the assembled capsid. Most viruses can be classified as rodlike or spherical, with the capsids of rodlike viruses arranged with helical symmetry around the nucleic acid, such as tobacco mosaic virus (TMV), and the capsids of most spherical viruses arranged with icosahedral symmetry. There are also important exceptions discussed below. The number of protein copies comprising a helical capsid is arbitrary and thus a helical capsid can accommodate a nucleic acid of any length. In contrast, icosahedral capsids are limited by the geometric constraint that at most 60 identical subunits can be arranged into a regular polyhedron. However, early structural experiments indicated that many spherical capsids contain multiples of 60 proteins.

Caspar and Klug proposed geometrical arguments that describe how multiples of 60 proteins can be arranged with icosahedral symmetry, where individual proteins interact through the same interfaces but take slightly different, or quasi-equivalent, conformations [43]. Protein subunits can be grouped into morphological units or ''capsomers,'' usually as pentamers and hexamers. Icosahedral symmetry requires exactly 12 pentamers, located at the vertices of an icosahedron inscribed within the capsid. A complete capsid is comprised of $60T$ subunits, where T is the ''triangulation number,'' which is equal to the number of distinct subunit conformations.

In brief, a structure with icosahedral symmetry is comprised of 20 identical facets. The facets are equilateral triangles and thus themselves comprise at least three identical asymmetric units (asu's). The only requirement of the asymmetric units is that they are arranged with threefold symmetry, although many capsid proteins have a roughly trapezoidal shape [44] and it has been argued that this shape is ideal for tiling icosahedral structures [45]. The Caspar–Klug (C–K) classification system can be obtained starting from a hexagonal lattice as shown in Fig. 1. An edge of the icosahedral facet is defined by starting at the origin and

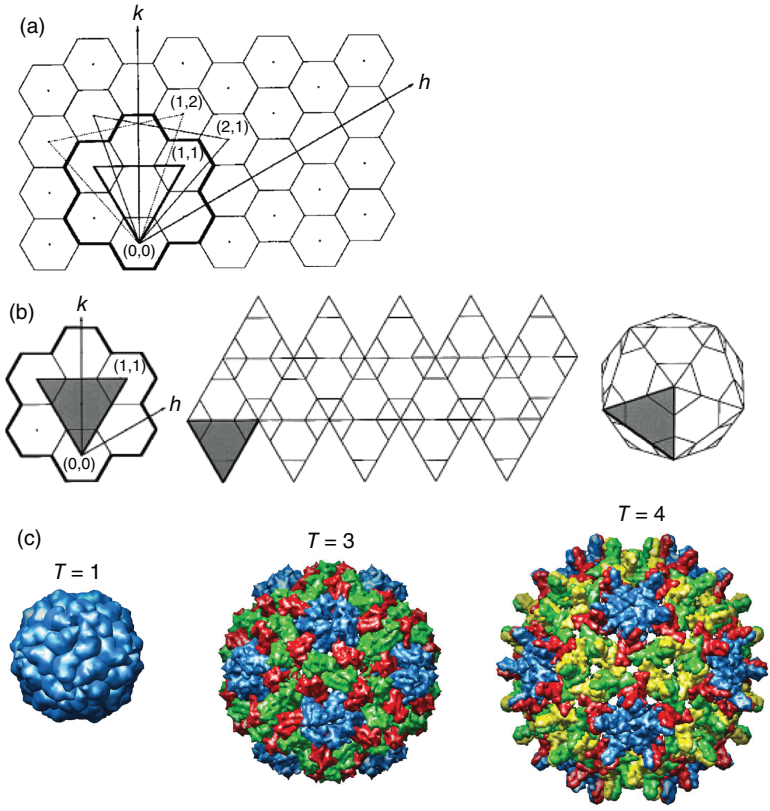

Figure 1. The geometry of icosahedral lattices. **(a)** Different equilateral triangular facets can be constructed on a hexagonal lattice by moving integer numbers of steps along each of the $\hat{\mathbf{h}}$ and $\hat{\mathbf{k}}$ lattice vectors. **(b)** Construction of a $T = 3$ lattice. Twenty copies of the triangular facet (left) obtained by moving one step along each of the $\hat{\mathbf{h}}$ and $\hat{\mathbf{k}}$ lattice vectors are arranged as shown in the middle panel, and then folded to obtain the icosahedral structure shown on the right. To connect this construction to a capsid, note that each pentagon will comprise 5 proteins in identical environments and each hexagon will comprise six subunits in two different types of local environments, resulting in a total of 180 proteins in three distinct local environments. **(c)** Example icosahedral capsid structures. From left to right are shown the $T = 1$ STMV capsid (PDBID 1A34) [46], the $T = 3$ cowpea chlorotic mottle virus (CCMV) capsid (PDBID 1CWP) [47], and the $T = 4$ human hepatitis B virus (HBV) capsid (PDBID 1QGT) [48]. Structures are shown scaled to actual size, and the protein conformations are indicated by color. In each image, the 60 pentameric subunits are colored blue. The images of capsids in **(c)** were obtained from the Viper database [41]. The images in **(a)** and **(b)** were reprinted from Ref. [49], with permission from Elsevier.

stepping distances h and k along each of the respective lattice vectors. There is an infinite series of such equilateral triangles corresponding to integer values of h and k. The area of such a triangle (for unit spacing between lattice points) is given by $T/4$, where T is the triangulation number defined as

$$T = h^2 + hk + k^2 \tag{1}$$

Considering that the smallest such triangle $T = 1$ comprises 3 asu's, the total number of asu's in the facet is thus given by $3T$ and the total number of asu in the icosahedron is $60T$. From Fig. 1, the individual asu's are not all identical for $T > 1$ since they have different local environments. Given the threefold symmetry of the facet, there are T distinct local environments and thus T distinct asu geometries. Figure 1b shows how to build a physical model for such a construction with $T = 3$.

The asu's (i.e., individual proteins) within the icosahedral structure can be grouped based on whether they sit at a fivefold or threefold (quasi-sixfold) axis of symmetry into pentameric or hexameric ''capsomers.'' Given that an icosahedron contains 12 vertices with fivefold symmetry and the total number of proteins is given by $60T$, there are $10(T - 1)$ hexamers.

Many icosahedral viral capsids with $T > 1$ are comprised of only a single protein copy, meaning that the protein must adopt different configurations depending on its local environment. It was originally proposed by Caspar and Klug [43] that because the local environments are similar, or ''quasi-equivalent,'' the proteins in different environments could interact through the same interfaces. This has since been found to be correct for many icosahedral viruses, with structural differences between proteins at different quasi-equivalent sites often limited to loops and N- and C-termini. However, there can also be proteins with extensive conformational changes or even different sequences at different sites. Some examples of these structural differences are reviewed in Refs. [49,50].

Some icosahedral virus capsid structures deviate from the class of lattice structures shown in Fig. 1. For example, the *Polyomaviridae* [e.g, human papilloma virus (HPV)] are comprised entirely of pentamer capsomers, which depending on their local environment are either fivefold or sixfold coordinated. Generalizations of the C–K classification scheme have been proposed [51–57], which can describe polyomavirus capsid shapes. Mannige and Brooks identified a relationship between hexamer shapes and capsid properties such as size [45,58]. They also developed a metric for complexity of icosahedral morphologies, which resulted in a ''periodic table'' of capsids and, combined with the assumption that the simplest structures are the fittest, revealed evolutionary pressures on capsid structures [59].

There are also nonspherical capsids with aspects of icosahedral symmetry. For example, the mature HIV virus capsid assembles into tubular or conical shapes [60–63] and some bacteriophages (viruses that infect bacteria) have capsids that

are elongated or prolate icosahedra (e.g., [64,65]). The C–K classification system was extended to describe prolate icosahedra by Moody [64]. We present some approaches to model the stability and formation of capsids that correspond to C–K structures or their generalizations in Section III.F.

B. Virus Assembly

Viral assembly most generally refers to the process by which the protein capsid(s) form, the nucleic acid becomes encapsulated within the capsid, membrane coats are acquired (if the virus is enveloped), and any maturation steps occur. For many viruses, the capsid can form spontaneously, as demonstrated in 1955 by the experiments of Fraenkel-Conrat and Williams in which the RNA and capsid protein of TMV spontaneously assembled *in vitro* to form infectious virions [66].

The pathway of nucleic acid encapsulation differs dramatically between viruses with single-stranded or double-stranded genomes. Viruses with single-stranded genomes (the best studied of which have ssRNA genomes) usually assemble spontaneously around their nucleic acid in a single step. This category includes many small spherical plant viruses (e.g., STMV or *Bromoviridae*), the bacteriophage MS2, and animal viruses such as nodavirus. In many cases, the RNA is required for assembly at physiological conditions, but the capsid proteins can assemble without RNA into empty shells *in vitro* under different ionic strengths or pH. We also can include in this group the *Hepadnaviridae* family of viruses (e.g., HBV), which have a dsDNA genome but a capsid that assembles around an ssRNA pregenome [67–69].

The extreme stiffness of a double-stranded genome (the persistence length of dsDNA is 50 nm) and the high charge density preclude spontaneous nucleic acid encapsidation. Thus, packaging a double-stranded genome requires a two-step process in which an empty protein shell is assembled followed by packaging via ATP hydrolysis and/or complexation with nucleic acid folding proteins (e.g., histones [70,71]). Of these viruses, the assembly processes have been most thoroughly investigated for dsDNA viruses, such as the tailed bacteriophages, herpes virus, and adenovirus. These viruses assemble an empty capsid, without requiring a nucleic acid at physiological conditions, and a molecular motor that inserts into one vertex of the capsid [72]. The motor then hydrolyzes cellular ATP to pump the DNA into the capsid.

In this chapter, we will focus on the assembly of icosahedral viruses, first discussing the assembly of empty capsids, such as that occurring during the first step of bacteriophage assembly, then co-assembly of capsid proteins with RNA, such as that occurring during replication of ssRNA viruses, and finally co-assembly with other polyanions in *in vitro* experiments. We will not consider the assembly of rodlike viruses. Although not yet completely understood, the assembly process

for the rodlike virus TMV has been studied in great detail and has been the subject of several reviews [73–75] as well as more recent modeling studies [76,77].

1. *Experiments That Characterize Capsid Assembly*

The kinetics for spontaneous capsid assembly *in vitro* have been measured with size-exclusion chromatography (SEC) and X-ray and light scattering (e.g., [78–85]). Most frequently, the fraction of subunits in capsids or other intermediates has been monitored using SEC and the mass-averaged molecular weight has been estimated with light scattering. The SEC experiments show that under optimal assembly conditions the only species present in detectable concentrations are either complete capsids or small oligomers, which we refer to as the basic assembly unit. The size of the basic assembly unit is virus dependent, for example, dimers for bromoviruses [86] and HBV [87,88] or pentamers for picornaviruses [e.g., human rhinovirus (HRV)] and the *Polyomaviridae* family [89] (e.g., HPV). Provided that intermediate concentrations remain small, the mass-averaged molecular weight and thus the light scattering closely tracks the fraction capsid measured by SEC. Example light scattering measurements from Ref. [79] are shown in Fig. 2a for HBV assembly at several ionic strengths.

While these bulk experiments have provided tremendous information about capsid assembly kinetics, it has been difficult to characterize assembly pathways in detail because the intermediates are transient and present only at low levels. Complementary techniques have begun to address this limitation. Restive pulse sensing was used to track the passage of individual HBV capsids through conical nanopores in a membrane [90,91]. This Coulter counter-like apparatus was able to distinguish between $T = 3$ and $T = 4$ capsids. Mass spectrometry has been used to characterize key intermediates in the assembly of MS2 by Stockley and coworkers [92–94] (see Section III.F.2) and for HBV and nodavirus by Uetrecht et al. [95]. Furthermore, fluorescent labeling of capsid proteins [96] and in some cases RNA has enabled measuring assembly timescales for capsids *in vivo* (reviewed in Refs. [97,98]).

2. *Motivation for and Scope of Modeling*

Even with the experimental capabilities to detect and characterize key intermediates for some viruses, theoretical and computational models are important complements to elucidate assembly pathways and mechanisms. Each intermediate is a member of a large ensemble of structures and pathways that comprise the overall assembly process for a virus. Furthermore, assembly is driven by collective interactions that are regulated by a tightly balanced competition of forces between individual molecules. It is difficult, with experiments alone, to parse these interactions for those mechanisms and factors that critically influence

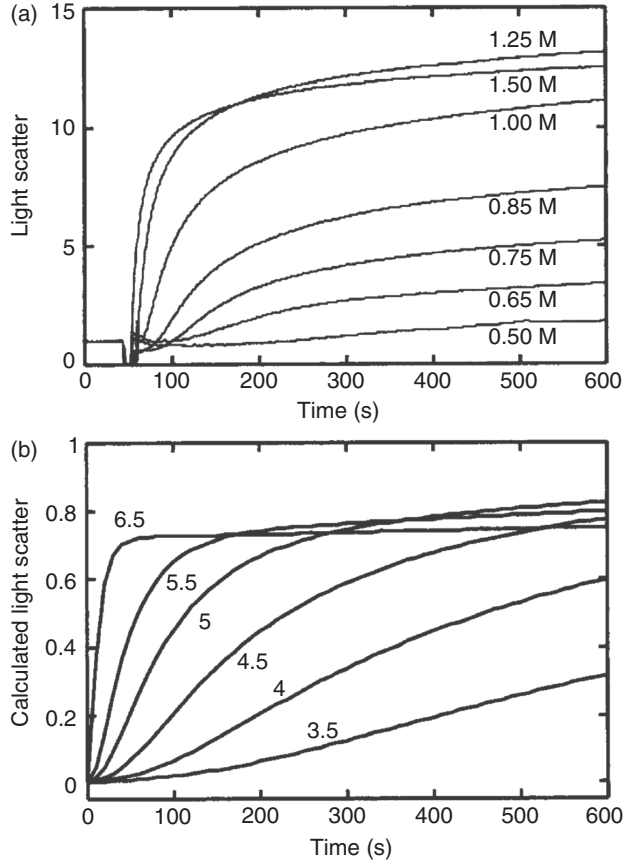

Figure 2. **(a)** Light scattering measured as a function of time for 5 μM dimer of HBV capsid protein at indicated ionic strengths. Light scatter is approximately proportional to the mass-averaged molecular weight of assemblages and, under conditions of productive assembly, closely tracks the fraction of subunits in capsids (see text). **(b)** Simulated light scattering for 5 μM subunit with indicated values of the subunit–subunit binding free energy (g_b) using the rate equation approach described in Section III.B. Figures reprinted with permission from Ref. [79], copyright (1999) American Chemical Society.

large-scale properties. With a model, one can tune each factor individually to learn its effect on the assembly process. In this way, models can be used as a predictive guide to design new experiments. However, whether at atomistic or coarse-grained resolution, models involve important simplifications or other inaccuracies in their

representation of physical systems. Thus, comparison of model predictions to experiments is essential to identify and then refine important model limitations. Iterative prediction, comparison, and model refinement can identify the key factors that govern assembly mechanisms.

The large ranges of lengthscale and timescale (Å–μm, ps–min) that are relevant to most capsid assembly reactions hinder simulating the process with atomic resolution, although Freddolino et al. [1] performed an all-atom simulation of the intact STMV. Recently, approaches to systematically coarse grain from atomistic simulations have been applied to interrogate the stability of intact viruses [2–4] or to estimate subunit positions and orientations from cryo-electron microscopy images of the immature HIV capsid [99]. All-atom molecular dynamics has been applied to specific elements of the assembly reaction [100]. As we describe below, most efforts to model capsid assembly to date have considered simplified models that retain those aspects of the physics that are hypothesized to be essential, with the validity of the hypothesis to be determined by comparison of model predictions with experiments.

II. THERMODYNAMICS OF CAPSID ASSEMBLY

We will begin our discussion of viral assembly by analyzing the formation process of an empty capsid. While this process is most relevant to viruses that first form empty capsids during assembly, ssRNA capsid proteins have also been examined with *in vitro* experiments in which the ionic strength and pH were adjusted to enable assembly of empty capsids.

A. Driving Forces

For assembly to proceed spontaneously, states with capsids must be lower in free energy than a state with only free subunits. The assembly of disordered subunits (and RNA or other components, if applicable) into an ordered capsid structure reduces their translational and rotational entropy, and thus must be driven by favorable interactions among subunits and any other components that overcome this penalty. We begin here with the protein–protein interactions; the subunit–RNA interactions that promote ssRNA capsids to assemble around their genome are discussed in Section IV and also reviewed in great detail by Siber et al. [34]. Capsid proteins are typically highly charged and possess binding interfaces that bury large hydrophobic areas. Thus, as with most protein–protein interactions [101], capsid assembly results from a combination of hydrophobic, electrostatic, van der Waals, and hydrogen bonding interactions. Covalent interactions typically

do not play a role in assembly, although they appear during subsequent maturation steps for a number of viruses (e.g., the bacteriophage HK97 [102]).

Importantly, all of these interactions are short-ranged under assembly conditions. van der Waals interactions and hydrogen bonds operate on length scales of a few angstroms. Electrostatic interactions are screened on the scale of the Debye length, $\lambda_D \approx 0.3/C_{salt}^{1/2}$, with λ_D measured in nanometers and the salt concentration C_{salt} measured in molar units. At physiological ionic strength, $C_{salt} = 0.15$ M, the screening length is $\lambda_D \approx 1$ nm; *in vitro* experiments typically occur within the 0.05–1 M range. The hydrophobic interactions are similarly characterized by a length scale of approximately 0.5–1 nm [100,103,104].

In many cases, the interaction is primarily driven by hydrophobic interactions, and attenuated by electrostatic interactions with directional specificity imposed by van der Waals interactions and hydrogen bonding at Å length scales. The importance of hydrophobic interactions and the sometimes antagonistic contributions of direct electrostatic interactions have been shown by measuring the dimerization affinity of the C-terminal domain of the HIV capsid protein under an extensive series of mutations to the dimerization interface [105–107]. Furthermore, Ceres and Zlotnick [87] showed that the thermodynamic stability of HBV capsids increases with both temperature and ionic strength. The increase in stability with temperature suggests that hydrophobic interactions are the dominant driving force [103]. The increase in stability with ionic strength, on the other hand, suggests that the salt screens repulsive electrostatic interactions that oppose protein association. Several models based on this hypothesis reproduce the dependence of protein–protein interaction strength on ionic strength measured in the experiments [34,76,108]. However, it is worth noting that the experiments were performed on capsid protein with the highly charged C-terminal domain truncated, and it is difficult to pinpoint on the crystal structure which charges are responsible for repulsive interactions. Ceres and Zlotnick [87] suggested that higher salt concentrations could enhance assembly by favoring a capsid protein conformation that is active for assembly.

B. Law of Mass Action

We now consider the assembly thermodynamics for subunits endowed with the interactions just described. We begin by considering the equilibrium for a system of identical protein subunits assembling to form empty $T = 1$ capsids. To make the calculation analytically tractable, we assume here that there is one dominant intermediate species for each number of subunits n; extending this assumption is conceptually straightforward. The word subunit refers to the basic assembly unit defined in Section I.B.1.

The total free energy F_{EC} for a system of subunits, intermediates, and capsids in solution can be written as

$$F_{\mathrm{EC}}/k_{\mathrm{B}}T = \sum_{n=1}^{N} k_{\mathrm{B}}T\rho_n \left[\log(\rho_n v_0) - 1\right] + \rho_n G_n^{\mathrm{cap}} \tag{2}$$

where v_0 is a standard state volume, ρ_n is the density of intermediates with n subunits, and G_n^{cap} denotes the interaction free energy of such an intermediate. A plausible model for the interaction free energy is

$$G_n^{\mathrm{cap}}(g_{\mathrm{b}}) = \sum_{j=1}^{n} (n_j^{\mathrm{c}} g_{\mathrm{b}}) - TS_n^{\mathrm{degen}} \tag{3}$$

where n_j^{c} is the number of new subunit–subunit contacts formed by the binding of subunit j to the intermediate, g_{b} is the free energy for such a contact, and S^{degen} accounts for degeneracy in the number of ways subunits can bind to or unbind from an intermediate (see the s factors in Refs. [109,110] and Fig. 3). These terms are specified by the geometry of the capsid. Here we have subsumed rotational binding entropy penalties into g_{b} (see Refs. [111–114]) and, to reduce the number of parameters, assumed that the binding energy g_{b} is the same for all contacts. As discussed in Section II.A, g_{b} depends on temperature, ionic strength, and pH. Equation (3) can be readily extended to allow for interface-dependent contact energies and subunit conformational changes [115].

To obtain the equilibrium concentration of intermediates, we minimize F_{EC} subject to the constraint that the total subunit concentration ρ_{T} is conserved:

$$\sum_{n=1}^{N} n\rho_n = \rho_{\mathrm{T}} \tag{4}$$

This yields the well-known law of mass action (LMA) result for intermediate concentrations [116,117]:

$$\begin{aligned} \rho_n v_0 &= \exp[-\beta(G_n^{\mathrm{cap}} - n\mu)] \\ \mu &= k_{\mathrm{B}}T \log(v_0\rho_1) \end{aligned} \tag{5}$$

with μ the chemical potential of free subunits and $\beta = 1/k_{\mathrm{B}}T$. Due to the constraint [Eq. (4)], Eq. (5) must be solved numerically. The result for a model dodecahedral capsid comprised of 12 pentagonal subunits is shown in Fig. 3 for several values of the binding energy g_{b}. Notice that in all cases the capsid protein is almost entirely

(a)

		Build				
n	Model	Up	Down	S_n	c	K'_n
1		–	–	–	–	–
2		5/2†	1	5/2	1	$e^{-1\Delta G/RT}$
3		2	3	2/3	2	$e^{-2\Delta G/RT}$
4		3	2	3/2	2	$e^{-2\Delta G/RT}$
11		2	5	2/5	4	$e^{-4\Delta G/RT}$
12		1	12	1/12	5	$e^{-5\Delta G/RT}$

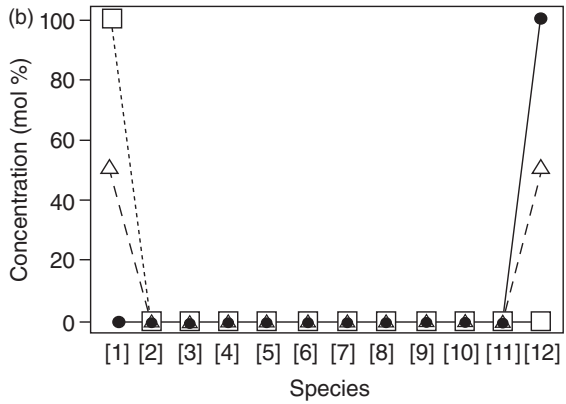

Figure 3. **(a)** The assembly model for a dodecahedral capsid and the statistical weights associated with symmetries for the intermediates. The columns list, respectively, the number of intermediates, the lowest energy configuration, the degeneracy for adding an additional subunit [s_n in Eq. (20)], the degeneracy for losing a subunit [$\hat{s}_n$ in Eq. (20)], the net degeneracy [S_n^{degen} in Eq. (3)], the number of contacts gained by adding a subunit [n_j^c in Eq. (3)], and the corresponding equilibrium constant. Only the first four and last two intermediates are shown; the full set is given in Ref. [109]. **(b)** The mole fractions of each intermediate calculated using Eq. (5) and the statistical factors in **(a)** are shown for total subunit concentrations ρ_T of 0.44 μM (□), 0.88 μM (△), and 1.8 μM (●). Figures reprinted with permission from Ref. [109], copyright (1994) Elsevier.

sequestered either as free subunits or in complete capsids. This prediction, which is analogous to the result for spherical micelles with a preferred diameter [116], is generic to any description of an assembling structure in which the interaction free energy G_n^{cap} is minimized by one intermediate size ($n = N$) and the total subunit concentration is conserved.

To emphasize the generic nature of the prediction that intermediate concentrations are negligible at equilibrium, we also consider a continuum model of an assembling shell presented by Zandi et al. [118]. Each partial capsid intermediate is described as a sphere, with a missing spherical cap. The unfavorable free energy due to unsatisfied subunit–subunit interactions at the perimeter of the cap is represented by a line tension σ, so the interaction free energy for a partial capsid with n subunits is

$$G^{\mathrm{cap}}(n) = ng_{\mathrm{s}} + \sigma l(n) - b \tag{6}$$

with the perimeter of the missing spherical cap given by

$$l(n) = 2\pi R \sin\theta(n) = v_0^{1/3} 2[\pi n(N-n)/N]^{1/2} \tag{7}$$

with $v_0^{1/3}$ the size of one subunit and g_{s} the binding free energy per subunit (not per contact) in a complete capsid. Finally, we have included $b = g_{\mathrm{s}} + 2\sigma l(1)$ to ensure that free subunits have no interaction energy, since the continuum model breaks down for small intermediates. We set the line tension to $\sigma = -g_{\mathrm{s}}/2$, which indicates that, on average, a subunit adding to the perimeter of the capsid satisfies half of its contacts. The resulting profile for $G(n)$ is shown in Fig. 4b, with the intermediate concentrations for several values of ρ_{T}/ρ^* shown in Fig. 4c. In all cases, the intermediate concentrations are negligible.

Two-state approximation. Based on the observation that intermediate concentrations are negligible at equilibrium, the equations for capsid assembly thermodynamics can be simplified considerably by neglecting all intermediates except free subunits or complete capsids, so that

$$\rho_{\mathrm{T}} = \rho_1 + N\rho_N \tag{8}$$

Defining the fraction of subunits in capsids as $f_{\mathrm{c}} = N\rho_N/\rho_{\mathrm{T}}$, combining Eqs. (5) and (8), and rearranging, we obtain [119]

$$\frac{f_{\mathrm{c}}}{1-f_{\mathrm{c}}} = N(v_0\phi_{\mathrm{T}})^{N-1} \mathrm{e}^{-\beta G_N^{\mathrm{cap}}} \tag{9}$$

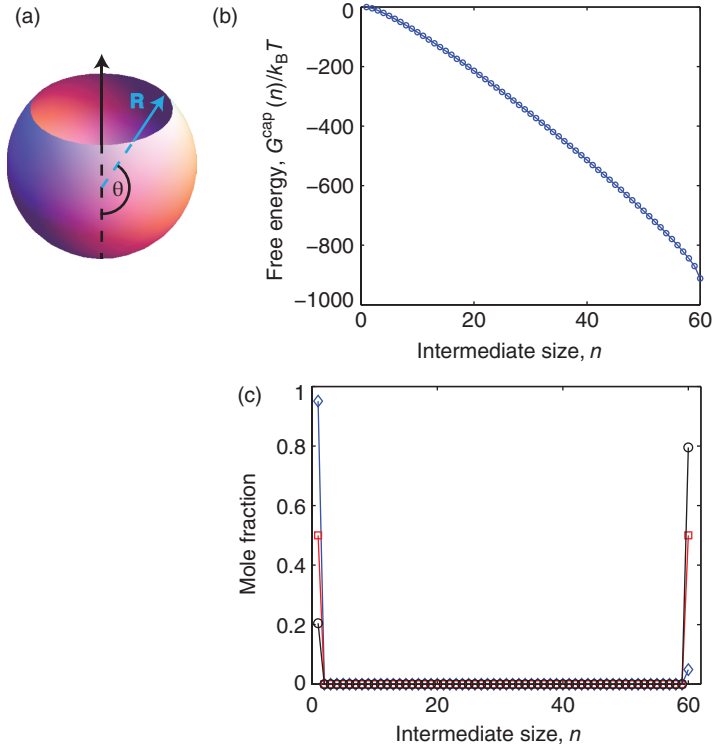

Figure 4. **(a)** Depiction of the continuum model description of partial capsid intermediates considered by Zandi et al. [118]. R is the radius of the capsid and the angle θ characterizes the extent of completion of the capsid. **(b)** Interaction free energy $G(n)$ as a function of intermediate size n obtained from Eq. (6). **(c)** Predicted mole fractions using Eqs. (4) and (6) for $\rho_T = \rho^*$ ($\diamond$), $\rho_T = 2\rho^*$ ($\square$), and $\rho_T = 5\rho^*$ ($\circ$). $g_s = -15k_BT$ for **(b)** and **(c)**.

In the limit $N \gg 1$, this gives

$$\frac{f_c^{1/N}}{1-f_c} = \frac{\rho_T}{\rho^*}$$

$$\rho^* v_0 = \exp\left(\beta \frac{G_N^{cap}}{N-1}\right) N^{-1/(N-1)} \approx \exp\left(\beta G_N^{cap}/N\right) \tag{10}$$

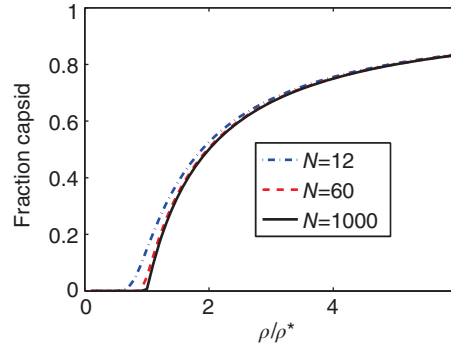

Figure 5. Fraction capsid f_c as a function of subunit oversaturation ρ/ρ^* predicted by Eq. (10) for the number of subunits in a complete capsid $N = 12$, 60, and 1000.

with ρ^* the pseudocritical subunit concentration. In the asymptotic limits, Eq. (10) reduces to

$$f_c \approx \left(\frac{\rho_T}{\rho^*}\right)^N \ll 1 \quad \text{for } \rho_T \ll \rho^*$$

$$\approx 1 - \frac{\rho^*}{\rho_T} \qquad \text{for } \rho_T \gg \rho^* \tag{11}$$

The solution to Eq. (11) is shown in Fig. 5 for several values of the capsid size N; note that the transition becomes sharper with increasing capsid size. Also notice that increasing the total subunit concentration ρ_T or the magnitude of the binding energy (i.e., decreasing ρ^*) always increases the fraction of subunits in complete capsids f_c at equilibrium. We will see, however, in Section III that this trend does not always apply at finite but experimentally relevant timescales due to kinetic effects.

Higher T numbers. If one or a few ground-state capsid geometries are known (or pre-assumed), the thermodynamic calculation described above can be extended to describe capsids with larger T numbers in a straightforward manner. Recalling from Section I.A that icosahedral capsids comprise T different subunit conformations (or in some cases protein sequences), the capsid free energy G_N^{cap} must be extended to include conformation energies and contact free energies g_b, which depend on the subunit conformation or species [115]. Approaches to determine the lowest free energy configuration(s) for a shell are discussed in Section III.F.1.

1. Estimating Binding Energies from Experiments

Ceres and Zlotnick have shown that the assembly of HBV [87] can be captured by Eq. (10) using g_b as a fit parameter (see Fig. 6). These fits yield an important

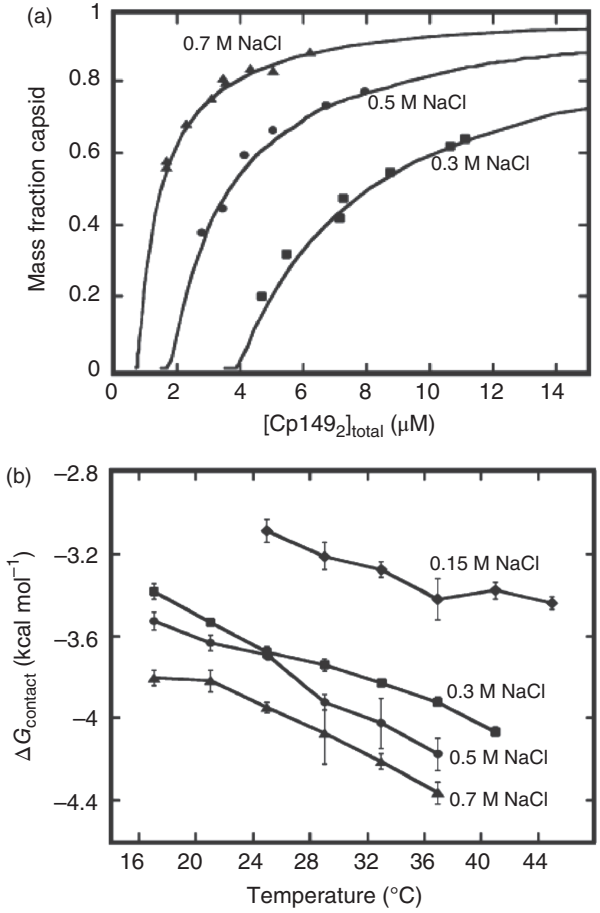

Figure 6. **(a)** Fraction capsid measured for assembly of empty HBV capsids from capsid protein in which the RNA binding domain has been truncated, Cp149, using SEC as a function of total dimer subunit concentration $[C_p149_2]_{total}$. Results are shown for indicated salt concentrations, and the lines are fits to the equilibrium model with $G_N^{cap} = 240g_b - T\log(s_N)$ assuming four contacts per subunit and using the contact energy g_b as a salt concentration-dependent fit parameter, with the symmetry number of the complete $T = 4$ capsid as $s_N = 2^{119}/120$ [87]. **(b)** Estimated values of g_b as a function of temperature and ionic strength. Reprinted with permission from Ref. [87], copyright (2002) American Chemical Society.

observation that the subunit–subunit binding free energies are quite small, on the order of $g_b = 4$ kcal/mol^{-1} ($6.7k_BT$) for productive assembly reactions. The observation that capsid assembly is driven by weak interactions of this magnitude appears to be a general rule for capsid assembly [120], for reasons discussed in Section III.

The conclusion that most of the interactions driving capsid assembly are weak appears to be broadly valid. However, it is important to note that Eq. (10) is an equilibrium expression, and thus strictly applies only on times exceeding any relevant reaction timescale. We can immediately see that this condition is beyond the reach of many experiments by estimating the timescale for a single subunit to leave an assembled capsid. Consider a typical subunit–subunit association rate constant of $f = 10^5$ M$^{-1}s^{-1}$ ([79,82,110], see Section III.B) and a typical binding free energy of $g_b = 6.7k_BT$. Since the dimer subunits of HBV are tetravalent, the first subunit must break four contacts to dissociate, with a timescale of about $t_{\text{dissociate}} \sim f \exp(4g_b/k_BT) = 50$ days. Similarly, we show in Section III.A.1 that the approach of assembly toward equilibrium must lead to ever-increasing nucleation barriers. Based on dynamical assembly simulations, our group has estimated that the values of g_b could be underestimated by about k_BT even for measurements taken at 24 h due to this effect.

The actual timescales for subunit dissociation from complete capsids can be estimated from experiments that labeled subunits to monitor exchange with complete P22 capsids [121] as well as $T = 3$ and $T = 4$ HBV capsids [122]. Subunit exchange on a period of days to months was indeed demonstrated for the P22 capsids and a fraction of the subunits in the $T = 3$ HBV capsids. However, no subunit exchange was observed for $T = 4$ HBV capsids, even when temperature was decreased to 4° C (recall that HBV is less stable at lower temperature). Similarly, Singh and Zlotnick [123] measured substantial hysteresis for the dissociation of HBV capsids under denaturant. These observations raise the possibility that there are some steps that are irreversible (at least on measurement timescales) in the assembly process. Irreversible steps late in assembly or during a post-assembly maturation process make sense from the perspective of virus replication, as they would extend the period of time over which the virus can remain complete in infinite dilution and unfavorable environments. Of course, there must be a mechanism to release the genome once the virus has infected a host.

The existence of irreversible steps cannot be directly revealed by assembly data alone. It has been shown that, even if there are assembly steps that are irreversible (on relevant timescales) late in the assembly cascade, as long as most steps are reversible the assembly data can be fit to Eq. (10) with an apparent value of g_b reflecting the free energy of the reversible steps [22,124–126]. Similarly, comparison of the dynamical equations described in Section III.B to kinetics data

could only reveal the presence of irreversible steps on timescales exceeding the equilibration time associated with the reversible steps (e.g., $\gtrsim$50 days).

III. MODELING SELF-ASSEMBLY DYNAMICS AND KINETICS OF EMPTY CAPSIDS

The experimental measurements of capsid assembly kinetics described in Section I.B.1 provide important constraints on models of capsid assembly kinetics. At the same time, they present an important opportunity for modeling; because only some intermediates can typically be characterized, models are essential to understand detailed assembly pathways. In this section, we describe different modeling approaches that have been used to predict or understand the assembly kinetics.

A. Timescales for Capsid Assembly

We begin our description of capsid assembly kinetics by defining the potential rate-limiting steps and presenting scaling estimates for their timescales. While our estimates are based on simplified models, we will see in the subsequent sections that many of the predictions remain applicable when additional details are accounted for.

It was noted by Prevelige et al. [78] that assembly kinetics for icosahedral capsids can be described in terms of nucleation and elongation (or growth) timescales, closely analogous to crystallization. Nucleation refers to formation of a ''critical nucleus'' or a structure that has a greater than 50% probability of growing to a complete capsid before disassembling (Fig. 7). Elongation then refers

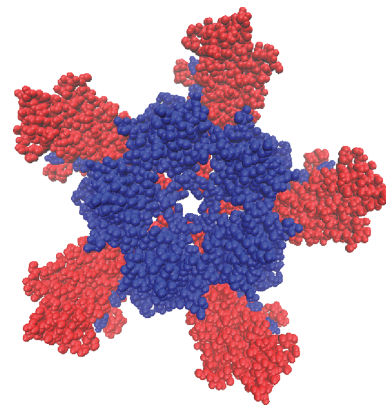

Figure 7. Image of the CCMV pentamer of dimers that experiments [80] indicate is the critical nucleus. Atoms are shown in van der Waals representation and colored according to their quasi-equivalent conformation, with A monomers in blue and B monomers in red. The coordinates were obtained from the CCMV crystal structure (PDBID 1CWP) [47] using the Viper oligomer generator [41] and the image was generated with VMD [127].